Pre-print version by the author
link to published article with DOI
J. Energy Chem. 2022, 68, 669-678
https://doi.org/10.1016/j.jechem.2021.12.034

Electrocatalytic production of glycolic acid from CO_2 via oxalic acid reduction on titania debris supported on a TiO_2 nanotube array

Francesco Pio Abramo[a], Federica De Luca[a], Rosalba Passalacqua[a], Gabriele Centi[a], Gianfranco Giorgianni[b], Siglinda Perathoner[a], Salvatore Abate[a,*]

[a] *Department of ChiBioFarAM (Industrial Chemistry), University of Messina, ERIC aisbl and INSTM/CASPE, V.le F. Stagno d'Alcontres 31, Messina 98166, Italy*

[b] *University of Calabria, Department of Environmental Engineering, Laboratory of Industrial Chemistry and Catalysis Via P. Bucci, 87036 Rende (CS), Italy*

Abstract

Electrodes prepared by anodic oxidation of Ti foils are robust and not toxic materials for the electrocatalytic reduction of oxalic acid to glycolic acid allowing to develop a renewable energy driven process for the production of an alcoholic compound from an organic acid at low potential and room temperature. Coupled with an electrochemical synthesis of the oxalic acid from CO_2 the process represents a new green and low-carbon path to produce added value chemicals from CO_2. Various electrodes prepared by anodic oxidation of Ti foils were investigated. They were characterized by the presence of a TiO_2 nanotube array together with the presence of small patches, debris or TiO_2 nanoparticles. A series of relationships between the characteristics of these samples, in particular the concentration of oxygen vacancies and the amount of Ti^{3+} detected by XPS or the intensity of the anodic peak in cyclic voltammetry tests, and the catalytic behavior (oxalic acid conversion and yield of glycolic acid) evidence the relation between these aspects. The analysis of the results indicate in small amorphous TiO_2 nanoparticles (or surface pathces or debris) stabilized by interaction with TiO_2 nanotubes the sites responsible for the conversion of oxalic acid and glycolic acid yield. By varying this structural characteristic of the electrodes, it is possible to tune the glycolic acid to glyoxylic acid relative ratio. A best cumulative Faradaic efficiency of about 84% with selectivity to glycolic acid around 60% and oxalic conversion about 30% was obserbed.

Key Words: Oxalic acid; TiO_2 nanotubes; glyoxylic acid; glycolic acid; electrocatalysis

*** Corresponding author.** Tel: +39-090-6765712; E-mail: abates@unime.it.

1. Introduction

The production of high-value chemicals by electrocatalytic reduction of CO_2 is one of the current challenges in energy chemistry to foster a fossil-free chemical industry based on the use of renewable energy resources [1-4]. While C1 products obtained by CO_2 reduction (CO, CH_3OH, formic acid) have a relatively low commercial value, enable the production of C2 and C3 (multicarbon) fuels and chemicals opens a range of novel and interesting possibilities from the industrial perspective (due to the higher added value) and thus can be considered the gate to deploy the electrocatalytic processes of CO_2 utilization [5-10]. However, the range of products which can be obtained by direct electrocatalytic reduction of CO_2 is relatively limited (main ethylene, ethanol and acetic acid/acetate). Alternatives to the direct reduction, a multistep path with the initial production of oxalic acid - OX (directly or indirectly via formic acid as intermediate) and then the electrocatalytic reduction of oxalic acid [5] along the paths drawn in Scheme 1 creates a new value chain [5]. Between the possible products, glyoxylic acid (GO) and glycolic acid (GC), which can be obtained from OX in a sequence of concerted two proton-electron transfer, are of special interest being high added-value chemicals, with an interesting potential market [5].

SCHEME 1 HERE

GC is used in several industries as an α-hydroxy acid: i) in the textile industry as a whitener and tanning agent, ii) in the food industry as a flavouring, iii) in the polymers industry as a monomer for the synthesis of polyglycolic acid (PGA), a biodegradable and thermoplastic polymer, or of poly (lactic-co-glycolic) acid (PLGA), as a copolymer that finds application in many therapeutic devices thanks to its biodegradability and biocompatibility [11]. GO is used in the production of pharmaceuticals, agrochemicals, and various food, personal care, and cosmetics components. GO and GC markets are forecast to reach together over one billion US$ by 2025. The product market value of GO and GC is around 4000 and 2000 €/ton, respectively, thus up to 2-3 times larger than the average for petrochemical intermediates. They are produced industrially with complex multistep processes. GC is produced, for example, either by a hydrative carbonylation of formaldehyde under very harsh reaction conditions or by chlorination of acetic acid and the subsequent hydrolysis of the resulting chloroacetic acid in the presence of sodium hydroxide. GO is produced by selective catalytic oxidation of GC and for this reason its commercial value is about twice that of GC. Thus, producing them from CO_2 by an electrocatalysis route could combine i) process intensification, ii) recycle of waste CO_2

and iii) introduction of renewables in the production chain. The electrocatalytic path from OX combines i) a potential cost reduction, ii) a reduced carbon footprint, iii) a process simplification (reduction and integration of steps), iv) the use of environmentaly more friendly industrial operations, v) the substitution of fossil fuels as raw material and vi) the use of renewable energy sources for the process. In other words, it is a good example of innovation towards a sustainable production. In addition, the current market for GO is strongly dependent on the cost and availability of GC being the raw material for GO. Producing GO from oxalic acid can thus decouple the two processes, although the electrocatalytic route has the great inherent advantage of allowing to produce both chemicals in the same equipment, and thus introduce also flexibility to better adapt to variable markets.

From an industrial perspective, the electrocatalytic route from oxalic acid as intermediate is thus quite attractive, and would be relevant to determine the conditions when GO or GC production could be maximized. The use of bio-based raw materials and catalytic or enzymatic processes represents an alternative possibility, but still the processes are at only the lab-scale development [12]. Note also that as remarked in Scheme 1, the route can be extended to produce in a sustainable process also other chemicals such as tartaric acid [13], besides to a range of valuable derivatives of GO and GC, not shown in *Scheme 1* for conciseness.

Earlier studies on the electrocatalytic reduction of OX use a lead cathode [14,15], but with the severe drawbacks of deactivation and that Pb is harmful both for the environment and humans [16]. To overcome these issues, alternative cathode materials more sustainable and with a better selectivity to GC or GO should be developed. However, literature data on this aspect are limited. The use of TiO_2 to replace the lead cathode was proposed by Masaaki et al. [17]. They used a porous anatase TiO_2 directly grown on a Ti mesh or Ti felt as cathode, but coupled with a costly IrO_2-based anode. GC was obtained with ~50% selectivity, while GO formed in minor amounts. Conversion of OX was also low (<15%) at the optimal applied voltage of 2.4 V. In addition, catalyst deactivated within one hour. These results are in contrast with earlier finding by Zhao et al. [18] that used a roughened TiO_2 film electrode prepared by anodic oxidation. They evaluated the behavior of these electrodes in a batch-type undivided electrochemical cell, applying high voltages (2.9-3.4 V). Even with the differences in conditions and type of electrocatalytic reactor, they observed GO rather than GC formation, with a maximum yield of about 57% after 8h at 3.3 V. The yield droped significantly when a Ti polished electrode rather than the roughened TiO_2 film electrode was used. This indicates that titania specific

characteristics likely determine the electrocatalytic behavior in OX reduction. This indication is supported by recent findings by De Luca et al. [19] showing that a composite electrode based on graphite-C_3N_4 decorating TiO_2 nanotubes is able to give a GC selectivity up to 76%, while pristine TiO_2 nanotubes are less selective (about 34%). The effect seems associated to the modification of the electronic structure of TiO_2 induced by the heterojunction with g-C_3N_4. Thus, TiO_2 appears as a promising material to develop cathodes for the electrocatalytic reduction of OX, but quite limited data are available in literature and indications about the specific role of titania, and how to optimize the electrocatalytic performances, are contrasting.

Here we thus aim to study the electroreduction of oxalic acid by using as cathode a TiO_2 film of well ordered and vertically aligned TiO_2 nanotubes (grown by anodic oxidation on a Ti plate acting as electrode conductive substrate; TiO_2NT/Ti) [20-25]. The advantage of this nanostructure is the good accessibility to the inner part of the nanotube even during the electrocatalytic reaction, due to the vertical-aligned structure and inner size of nanotubes in the 50-100 nm range. Thus, a high active (accessible) surface (a 3D-like electrode) can be obtained with respect to a TiO_2 layer obtained by compact TiO_2 nanoparticles. In addition, due to this nanostructure an enhanced electrical conductivity is induced with respect to a thin titania film of equivalent thickness [26]. Finally, the electrode results robust and easy scalable for industrial applications.

However, the specific characteristics of the electrode [27-29] depend largely on the details of the method of preparation. We have thus selected here for this study TiO_2NT/Ti electrodes prepared by different modalities (as described later), in order to tailor the characteristics of these electrodes. They were compared as benchmarking with TiO_2 (unordered) nanotubes prepared by hydrothermal synthesis and then deposited over the Ti substrate [30,31]. By comparing the physico-chemical and reactivity characteristics of TiO_2NT/Ti electrodes, with respect to benchmarking electrodes, it is thus possible to understand better the nature of the titania species involved in the electroreduction of OX and the factors allowing to tune the performances and selectivity, operating at the same time at significantly lower applied potentials than what reported in earler studies (around-1.1 vs Ag/AgCl), an important aspect in terms of exploitability of the results. Nanostructured TiO_2 electrodes find application in a range of energy uses, from DSSC cells to batteries, besides that as robust electrodes for electrochemical applications [32-36]. The study can be thus relevant for the entire field of titania-based electrodes as advanced energy materials.

The work here is focused for clarity only on the electrocatalytic OX reduction to GO and GC, but the other aspects outlined in Scheme 1, in particular the direct and indirect paths of OX formation from CO_2 are also investigated as part of the EU project OCEAN (Oxalic acid from CO_2 using Eletrochemistry At demonstratioN scale, project 767798) aimed to develop at a demo scale a new value chain in producing C2 chemicals from CO_2.

2. Experimental

2.1 Preparation of the electrocatalysts

TiO_2 nanotubes were synthesized by controlled anodic oxidation of titanium foils (Alfa Aesar) and of a commercial P25 Degussa TiO_2 under hydrothermal conditions. The first method leads to a self-ordered array (ordered hexagonal closely packed) of vertically-aligned TiO_2 nanotubes - TiO_2 NT, grown directly on the Ti foil acting as electron-conductive substrate for the electrode. Changes in the procedure lead to different electrodes, as described in section 2.1.1. The second (hydrothermal) method leads to the formation of a powder formed by not-ordered overlapping TiO_2 nanotubes. This powder is then deposited over the Ti foil to prepare the electrode.

2.1.1 Anodic Oxidation of Ti Foils

Ti foils (Alfa Aesar, diameter 35 mm, thickness 0.025 mm, purity 99.96 %), were oxidized a) as received or b) after pre-calcination at 450 °C for 30 min. Before the anodic oxidation procedure, all the Ti foils were washed sequentially for 10 min in i) distilled water, ii) acetone, and iii) isopropyl alcohol, by using a ultrasonic bath. Anodic oxidation of washed Ti foils was carried out at r.t. for 1 hour in a two-electrode configuration cell equipped with a glassy carbon cathode, employing a constant applied potential of 50 V, using an aged electrolyte solution of NH_4F (0.3 wt % - Sigma-Aldrich, ≥ 98%), deionized water (2 wt %), and ethylene glycol (98 wt % - Sigma-Aldrich, 99.8%). The obtained TiO_2 nanotubes were rinsed by deionized water to remove the residual electrolyte and dried overnight. Finally, the dried TiO_2 nanotubes were calcined at 450 °C for 3 h with a temperature ramp of 2 °C/min.

By using the above-reported procedure, a set of three catalysts was prepared (Table 1). The TiNT and TiNT-A electrodes were prepared by varying the aging time between 60 and 240 min. Aging time is the time in which the electrolyte remains in contact with the electrode before to apply the potential of 50 V. In both cases, only cleaned Ti-foils were used. In the TiNT-T electrode case, the Ti foil was instead pre-calcined at 450°C (30 min).The other aspects of the

procedure remained unchanged.

TABLE 1 HERE

2.1.2 Hydrothermal catalyst synthesis

0.46 g of Degussa P25 TiO_2 (purity 99.9%, 85% Rutile and 25% Anatase, surface area 50 m^2/g, pore volume 0.11 cm^3/g, density 4.26 g/cm^3) were dispersed in 65 mL of 10 M NaOH solution, by using a ultrasonic bath for 15 minutes. The resulting suspension was hydrothermally treated in a Teflon-lined stirred autoclave at 130 °C for 24 h with a stirring rate of 600 rpm. The hydrothermally treated sample was filtered, rinsed with distilled water and treated with 0.1 M HCl under vacuum till neutral pH was reached. Then, it was protonated at r.t. in 0.1 M HCl under stirring (600 rpm) for 1 h. The protonated sample was rinsed with distilled water till neutral pH, dried at 80 °C overnight, and grounded. The resulting powder was dispersed in methanol (10 mg/ml) and deposited on a Ti foil using an airbrush (ABEST TJ-180K) to reach a theoretical TiO_2 loading of 1.5 mg/cm^2.

The as-prepared sample was dried at 80 °C overnight and, finally, calcined at 450 °C for 3 h (2°C/min), obtaining an experimental TiO_2 loading of 0.7 mg/cm^2. The prepared catalyst is referenced as TiNT-HS hereinafter (Table 1).

2.2 Experimental apparatus and electrodes testing procedure

The electrodes indicated in Table 1 were tested as cathodes in the electrocatalytic reduction of oxalic acid (OX) using the apparatus presented schematically in the Supplementary Info (Figure S1). The electrocatalytic cell uses a proton-exchange membrane (Nafion® 115) at the interface between the anodic (1) and cathodic (2) compartments and two external reservoirs for catholyte and anolyte. A 0.03 M OX solution (pH=2), containing a 0.2 M Na_2SO_4 solution was used in the cathodic compartment. In the anodic compartment, a 0.2 M Na_2SO_4 electrolyte solution was used. The pH of the anodic electrolyte solution was adjusted by adding controlled amounts of a 1 M H_2SO_4 solution until obtaining the same pH of the catholyte. A peristaltic pump was used to circulate the electrolytes. The volume of the electrolytic solution (cathode + external tank + tubes) was 35 ml, while 7 ml the net volume of the electrolyte in the electrocatalytic cell.

The amperometric detection experiments (AD) were performed at constant applied potential, in the range between -1.1 to -1.3 V at 25 °C, and monitoring the current density by an Amel potentiostat/galvanostat (Model 2551) for 2 h. All potentials were measured with respect to Ag/AgCl while H_2 was generated in situ by water co-electrolysis. A Metrohm 940 Professional

ionic chromatograph, equipped with a column for organic acids, was used to determine the concentration of the products formed at the cathode side of the electrocatalytic cell.

The following equations are used to express the electrocatalytic reactivity:

$$Faradaic\ efficiency\ (\%) = \frac{m_{product} * n * F}{Q}\ x\ 100$$

where $m_{product}$ represents the moles of the reduction products; n represents the number of electrons required for the formation of GO and GC from OX (n = 2 and 4 for the formation of GO and GC, respectively); F is the Faradaic constant (96485 C·mol^{-1} of electrons); Q is the total charge in Coulombs passed across the electrode during the electrolysis.

Oxalic acid conversion in electro-reduction experiments was defined using the following equation:

$$\text{Oxalic acid conversion } (\%) = \frac{[OX]i - [OX]t}{[OX]i}\ x\ 100$$

where $[OX]_i$ is the initial oxalic acid concentration and $[OX]_t$ is the oxalic acid concentration after 2h of reaction time.

The yield (Y) of the product is calculated

$$\text{Yield to } m_{product}\ (\%) = \frac{[M]t}{[OX]i}\ x\ 100$$

where $[M]_t$ is the concentration of $m_{product}$ after 2h of reaction time. [OX], [GO] and [GC] are the molar concentrations of OX, GO and GC, respectively.

2.3 Characterization methods

An XL-30 field emission scanning electron microscope (FEI/Philips), equipped with a High-Brightness Field Emission Gun (FEG) working at 3 kV, was used to investigate the nanostructure of the electrodes prepared.

PHI VersaProbe II (Physical Electronics), equipped with an Al Kα (1486.6 eV) X-ray source, measured the XPS spectra. The survey spectra were recorded with an analyzer energy path of 117 eV, while the C1s, O1s, and Ti2p core levels were measured at 23.5 eV. The X-ray beam size was 100 microns at 25 W. A charge neutralization procedure was performed by simultaneous irradiation of samples using a low-energy electron beam and an ion beam before measuring the spectra. The position of the XPS peaks was referenced to graphite carbon (284.8

eV). XPS peaks were deconvoluted using the Multipack Data Reduction Software (ULVAC-PHI, Inc), employing a Shirley background curve.

A potentiostat/galvanostat (Amel 2551) measured the cyclic voltammetry (CV) curves of the prepared electrocatalysts, both in the presence and in the absence (blank) of Oxalic acid (OX) as substrate. All the samples were measured using a 0-2 V potential (with respect to Ag/AgCl electrode) and a scan rate of 50 mV/sec, using the apparatus reported in Figure S2. Before CV measurements, the electrochemical cell was purged with Argon (20 ml/min) for 30 minutes.

Surface area of self-supported thin films was determined by the physical adsorption of N_2 onto the surface of the samples at liquid nitrogen temperatures by using a Autosorb IQ_3 sorption analyzer (Quantachrome) system.

3. Results

3.1. Characteristics of the samples prepared by anodic oxidation of Ti foils

3.1.1. Anodic Oxidation Curves

To illustrate the differences in the characteristics of the preparation of the three samples synthetized by anodic oxidation of Ti foils (see Table 1 for a summary), Figure 1 reports the anodization curves of current measured versus time of anodization.

FIGURE 1 HERE

TiNT and TiNT-A were prepared following the same anodization procedure, but changing the aging time. TiNT-T electrode instead is prepared as TiNT sample, but the Ti-foil is precalcinated before the anodization procedure. These relatively minor differences induce, however, significant changes in the anodization process (Figure 1). To describe better the differences, it is necessary to introduce shortly the mechanism of formation of the TiO_2 NTs.

The formation of TiO_2 NTs in the anodization process occurs through the simultaneous action of a) the electrochemical oxidation of Ti to TiO_2 (eq. 1) and b) the F^- driven chemical dissolution of TiO_2 (eq. 2), both induced by the electric field [37].

$$Ti + 2H_2O \rightarrow TiO_2 + 4H^+ \quad (1)$$

$$TiO_2 + 6F^- + 4H^+ \rightarrow [TiF_6]^{2-} + 2H_2O \quad (2)$$

The mechanism and description of the steps in the anodization curves is well established

through the following mechanism [38,39]:

1. Formation of dense non-conductive oxide layer on the surface of Ti foils, which causes a sudden lowering of the current followed by a lower rate of current decrease that marks the beginning of pore nucleation till the current minimum is reached (I_{min}).
2. Generation of the pores inducing an increase in the current due to the dissolution of the oxide till the maximum current is reached (I_{max}).
3. Growing of the nanotubes, characterized by a slow decrease of the measured current, due to the unbalance between the oxidation (eq. 1) and dissolution (eq. 2) steps.
4. A final step, when the nanotubes no longer grow, where the current remain stable or show a slow decrease due to the formation of irregular oxide particles (debris) on the top surface of the nanotube ordered array.

The TiNT sample, prepared with an aging time of 60 min using the only-cleaned Ti foils, shows an initial current (I_0) of 0.075 A, with a rapid decrease of the current in the first 120 s with a minimum (I_{min}) and maximum current (I_{max}) of about 0.0124 A and 0.0241 A shown at 120 s (t_{min}) ad 480 s (t_{max}), respectively. After 480 s only a small drop in the current was determined up to the end of the anodization procedure (final current 0.0234 A).

The sample with longer aging time (240 min, TiNT-A) shows an I_0 ~30% lower than that of TiNT, but the current decrease upon potential (50 V) application has a similar slope in TiNT-A and TiNT cases. However, I_{min} is significantly lower in TiNT-A with respect to TiNT, and also the time at which the minimum is obserbed shifts to 470 s (t_{min}). The current increases after the minimum is much less pronounced that TiNT case and a final current of about 0.046 A is reached after 1800 s. No I_{max} could be clearly identified in this case. Thus, TiNT and TiNT-A shown an initial processes of titania layer formation similar (eq. 1), but the reaction leading to NTs formation (eq. 2) is quite different, and less effective in TiNT-A, as well as the stage of debris formation could be not differentiated from that of NTs growth.

TiNT-T behavior is different. I_0 was 10% lower than that of TiNT, but current decreases upon potential application much less sharply, reaching t_{min} after 570 s (I_{min} of 0.022 A). Then, the current slowly continuously increases up to the end of the test, also without showing a maximum (I_{max}). In the case of TiNT-A, both the decreased I_{min} and I_{max} compared with the TiNT sample could be related to a lower rate of pore nucleation and nanotubes growth, due to the depletion of F^- ions in the electrolyte solution, aged for a longer time (240 min) with respect

to TiNT case (60 min). In TiNT-T case, the initial less sharp decrease in the current derives from an initial thin TiO_2 film formed during pre-oxidation, limiting the exposition of metallic Ti and affecing both the reactions reported in Eq.s 1 and 2. The presence of an oxide pre-layer, formed during the precalcination step, inhibits partially the formation of cracks/pits with exposed Ti, where the stronger electrical field induces the TiO_2 NTs formation.

Thus, the different trends of the anodization curves for TiNT, TiNT-A and TiNT-T electrodes can be well described based on literature indications [37-39]. What relevant here, however, is that the samples selected for this study can be well representative of different situations obtained in the formation of the ordered array of TiO_2 nanotubes and titania debris on it.

3.1.2. Scanning Electron Microscopy

The SEM top-view micrographs of the electrodes prepared by anodic oxidation are reported in Figure 2 (a-c for TiNT, TiNT-A and TiNT-C, respectively). Also the SEM micrograph of the sample of TiO_2 nanotubes prepared by hydrothermal treatment and deposited then on Ti foil (TiNT-HS) is reported for comparison.

FIGURE 2 HERE

Figure 2a shows the surface of TiNT, evidencing the presence of the ordered array of vertically-aligned TiO_2 NTs partially covered on the surface by TiO_2 debris. The TiO_2 nanotubes are well compact and dense with inner diameter ranging from 50 to 100 nm, and wall thickness about 15-20 nm. Figure 2b shows the top-view pf TiNT-A electrode evidencing the presence of a surface compact oxide layer without the apparent presence of an undelaying TiO_2 NTs array. This is consistent with the anodization curve due to the depletion of F^- ions in the aged electrolyte solution [38,40]. Figure 2c shows the top-view of the TiNT-T electrode, where the underlaying TiO_2 NTs array is well evidenced, but covered on the surface by large porous oxide patches, more compacts with respect to debris present in TiNT. In the TiNT-T case, with respect to TiNT, TiO_2 NTs shows a more uniform inner diameter (ranging from 40 to 60 nm) and also a thinner wall thickness (around 10nm), but a slightly less density of TiO_2 NTs packing. Figure S2 in the Supplementary Info reports an additional view of the TiNT-T sample, after cracking of the layer to reveal better the presence of an highly ordered and aligned vertically array of TiO_2 NTs with homogeneous dimensions and a well-defined structure. The results are consistent with indications given by Macak et al. [41] reporting an improved ordering of the tubes by using pre-structured surfaces. In our case, the thermal pretreatment creates the

initiation sites for TiO_2 NTs growth during the anodization process, leading to the more defined nanostructure with respect to TiNT, although the presence of large TiO_2 patches rather than debris as in TiNT, are observed.

The titania film thickness in all TiNTs samples ranges in the 0.7-0.8 μm range.

The SEM micrographs of the TiNT-HS sample (Figure 2d) show the presence of nanosheets (blue circles) and tubular nanostructures randomly oriented (see inset), in agreement with Moazeni et al. [42] also reporting similar indications. The packing of these TiO_2 nanosheets and nanotubes is less dense with respect to TiNT samples and some TiO_2 debris could be observed.

3.1.3. Cyclic Voltammetry

In order to characterize the differences between these samples and the impact on redox behavior, the electrodes were studied by cyclic voltammetry (CV) [43-46]. Figure 3a shows the voltammograms measured in a 0.2 M Na_2SO_4 solution (blank solution) for all the investigated samples. A reversible reduction peak at -1.26 V was observed for all samples and related to the reduction of Ti^{4+} to Ti^{3+} according to eq. 3:

$$TiO_2 + H_2O + H^+ + e^- \leftrightarrow Ti(OH)_3 \quad (3)$$

At -1.60 V starts the formation of gaseous hydrogen according to the eq. 4:

$$2H^+ + 2e^- \rightarrow H_2 \quad (4)$$

The negative current in this region is related to this reaction. The proton insertion-coupled electron transfer reaction occurs in parallel (eq. 5) [46]:

$$TiO_2 + xe^- + xH^+ \leftrightarrow Ti^{IV}_{1-x}T^{III}_x\,(O)_{1-x}(OH)_x \quad (5)$$

The decomposition of this product gives rise to the anodic peak around -1.5 V. For all the samples, an anodic peak in the range -0.8 ÷ -0.9 V is also observed and attributed to the oxidation of Ti^{3+} to Ti^{4+}. The peak intensity follows the order TiNT-T > TiNT-HS > TiNT > TiNT-A, suggesting the presence of larger amount of Ti^{3+} species in the TiNT-T sample. Quantification and correlation of these results with other characterization aspects will be discussed later.

FIGURE 3 HERE

In the presence of oxalic acid 0.03 M (Figure 3b), the anodic peaks become much less intense,

due the decreased oxidation of Ti^{3+} species, while the cathode current slightly increased.

The decreased intensity of such anodic peaks in oxalic acid solution suggests that the electrogenerated Ti^{3+} species reduces oxalic acid, in agreement with Zhao et al. [18] who observed a similar behavior on rough TiO_2 layer. In order to confirm this interpretation, a CV profile was performed on the TiNT sample by using a high concentration of OX (0.1 M), see Figure S3 (Supplementary Info). A higher cathode current was observed in the latter case, while the oxidation peak totally disappeared, confirming the electroreduction of OX by the electrons generated by the Ti^{3+}/Ti^{4+} redox couple.

These results indicate that the nanoporous TiO_2 film electrode acts as a good heterogeneous redox catalytic electrode, and oxalic acid undergoes fast chemical electroreduction.

3.1.4. X-ray photoelectron spectroscopy

The surface characteristics of TiNT electrodes were investigated by photoelectron spectroscopy. The survey spectra (Figure S4 in the Supplementary Info) indicate that TiO_2 nanotubes contain mainly Ti and O elements while no other impurities, except (as normal) the contamination by carbon (C1s peak). Other survey spectra, not reported for conciseness, shows similar features.

The high resolution XPS spectra were measured for Ti2p and O1s. The Ti2p core level spectra are reported in Figure S5 (Supplementary Info) for all the samples investigated. Ti2p spectra are deconvoluted in two peaks, the doublet Ti2p3/2 at 458.50±0.1 eV and Ti2p1/2 at 464.04±0.1 eV that are consistent with Ti^{4+} in TiO_2 lattice [47]. The shoulder peaks located at 456.91±0.1 eV and 462.45±0.1 eV are assigned to Ti2p3/2 and Ti2p1/2 and correspond to Ti^{3+}species in Ti_2O_3 [48]. The Ti2p1/2-Ti2p3/2 splitting energy was 5.54 eV.

All the high-resolution O1s core level spectra, reported in Figure 4, exhibit an asymmetric curve and a narrow shoulder, indicating the presence of a larger concentration of oxygen species in the near-surface region [49]. The O1s spectrum of each sample is deconvolved into two asymmetrical peaks named O1 and O2. The intense O1 peak, shown at 529.81±0.2, was attributed to the oxygen contained in the TiO_2 crystal lattice, while the O2 peak at 531.32±0.2 is attributed to the oxygen vacancy-Ti^{3+} surface state, also known as Ti_2O_3 [50].

FIGURE 4 HERE

The binding energy and the percentage of Ti^{3+} and O2 species calculated by using the Multipack software are reported in Table 2. Although the percentage of Ti^{3+} slightly changes in all the

samples, a linear correlation with the amount of O2 oxygen vacancies can be observed, as discussed later.

TABLE 2 HERE

3.1.5. Structural analysis and other characterizations of the electrodes

Characterization of the crystalline titania phases present in TiNT electrodes was made by glancing angle X-ray diffraction (GAXRD) measurements. The results were well consistent with previous results also supported by high resolution transmission electron microscopy [25] showing the presence of only TiO_2 anatase phase in samples annealed at 450 °C, while reflections due to TiO_2 rutile phase, in addition to those for the TiO_2 anatase phase, appear at annealing temperature of 500 °C or higher (Figure S7b in Supplementary Info). HRTEM characterization of the sample annealed at 450 °C [25] shows that the structure at the top is still characterized by a crystalline TiO_2 anatase structure, while the TiO_2 rutile phase is present at the bottom of the NTs, at the interface with the metallic Ti layer (Figure S6 in Supplementary Info). The titania patches or debris at the surface of the TiO_2 NTs ordered array results instead amorphous.

For TiNT-HS (sample prepared by hydrothermal synthesis), following the calcination at 450°C, well defined lines for crystalline TiO_2 anatase are present (Figure S7a in Supplementary Info).

Surface area measuraments obtained by physical adsorption of N_2 on the samples at liquid nitrogen temperatures (BET method) indicates a surface area in the 50-60 m^2/g range for all TiNT samples.

3.2. Electrocatalytic performances in oxalic acid reduction

Figure 5 shows the Faradic efficiencies (FE) to GO (glyoxylic acid, FE_{GO}) and GC (glycolic acid, FE_{GC}) and the OX (oxalic acid) conversion after 2 hours of electrocatalytic tests at three applied potentials (-1.1, -1.2, and -1.3 V). All samples were tested with an OX concentration of 0.03 M. The experimental setup is showed in Figure S1 (Supplementary Info)

The electrocatalytic performances can be lumped in two groups:

i) TiNT and TiNT-A showing low OX conversion (< 10%) and predominant formation of GO with respect to GC, but lower cumulative FEs (FE_{GO} + FE_{GC}) in TiNT-A with respect to TiNT (the difference is in H_2 side formation).
ii) TiNT-T and TiNT-HS samples, showing about three times higher OX conversion with

respect to the first group of electrodes, and also greater FE_{GC} with respect to FE_{GO} (with also higher global efficiency, FE_{GC} + FE_{GO} with respect to the first group of electrodes).

Performances are minor affected from the variation in the applied potential. At the optimal applied potential of -1.1 V, the FE_{GC} is equal to 58.3% and 60.8 % for TiNT-T and TiNT-HS, respectively.

FIGURE 5 HERE

For all the samples, the OX conversion is similar at each potential investigated, and the average value is reported in Table 2. It can be noted that the conversion increases from about 7% (for TiNT and TiNT-A) to 26% and 32%, respectively, for TiNT-HS and TiNT-T. The complete set of electrocatalytic results, including as comparison, also with the Ti foil after oxidative pretreatment at 450°C (30 min) (Ti-T), i.e. the same pretreatment used for TiNT-T electrode before the anodic oxidation, is reported in the Supplementary Info (Table S1). Not reported in Table S1 is the behavior of the Ti foil substrate, resulting fully inactive in GO or GC synthesis. After the pre-oxidation treatment (Ti-T), some activity is observed, but largely inferior than that of the electrodes prepared by anodic oxidation, due to the lower amount of nanostructured titania. These data confirm the role of TiO_2 as the electroactive element.

The removal of the surface TiO_2 amorphous patches or debris by ultrasonic treatment [51,52] do not lead to improvements in the performances, but rather to a minor or even negative effect (Figure S8 in Supplementary Info).

4. Discussion

4.1. Relationships between characteristics and reactivity of the electrodes

A series of linear relationships were observed between the features of the electrodes determined by the characterization methods discussed before and the electrocatalytic reactivity. The results are summarized in Figure 6.

FIGURE 6 HERE

A linear correlation is present (Figure 6b) between the intensities of the O2 peaks (attributed to oxygen vacancy) and the quantification of Ti^{3+} species by XPS analysis. Being present TiO_2 in the form of NTs array and amorphous oxide dense layer (TiNT-A), patches (TiNT) or debris (TiNT-T, TiNT-HS), while the ordered NTs array not present in the TiNT-A sample (while in

a different form in TiNT-HS), it may be concluded that the oxygen vacancies (O2) are associated to the formation of reduced Ti ions (Ti^{3+}) in amorphous TiO_2. Small debris are present, stabilized by the underlaying TiO_2 NTs array, are easier reducible and thus an higher amount of them is detected in TiNT-T, followed by TiNT-HS. More compact patches or layers result instead less reducible. This interpretation is well supported by the correlation obserbed between the anodic peak intensity obtained by CV (cyclic voltammetry, Figure 3) and O2 concentration measured by XPS (Figure 6c). The O2 concentration also linearly correlate with the average OX conversion (Figure 6a). The reducibility of small oxide TiO_2 nanoparticles resulting stabilized by the interaction with TiO_2 NTs, is thus the key to improve the reactivity in these electrodes.

Note, however, that the regression line does not pass through zero. This indicates that there is a fraction of oxygen vacancies (O2) results essentially inactive, possibly because located at the interface between the TiO_2 NTs and the Ti substrate, and thus largely unaccessible for the electrocatalytic activity.

In terms of GC synthesis, a nearly linear relationship could be also observed between the yield of GC (Y_{GC}) with respect to the fraction of oxygen vacancies (O2) (Figure 7). The relationship is less accurate with respect to those observed between O2 and Ti^{3+}, OX conversion (OX $Conv_{avg}$ reported in table 2) and Ipa (Figure 6). In addition, deviations from linearity are obserbed at lower applied potential, but where the average current density are lower with a conseguent higher error estimations, which is ± 8% on the average. Nevertheless the slightly less accurate relationship reported in Figure 7 indicate reasonably that also the yield to GC (GO is the only other product of OX reduction detected, except minor traces of other products indicated in Scheme 1) well correlate to the same active species discussed in relation to analysis of data in Figure 6, e.g. small oxide TiO_2 nanoparticles, easily reducible and stabilized from the interaction with TiO_2 NTs.

FIGURE 7 HERE

4.2. Nature of the active species for the selective electroreduction of OX to GC

Discussion in the previous section, and relationships evidenced in Figure 6a and 7 regarding OX conversion, yield of GC and concentration of oxygen vacancies (O2) and related correlation with reducibility of the electrode (amount of Ti^{3+} by XPS and intensity of the anodic peak in

CV experiments) evidence a clear correlation between reactivity and redox properties. By the analysis of the different electrodes investigated, the data evidence that small oxide TiO_2 nanoparticles (small patches or debris) are responsible for the electrocatalytic behavior, due to their easily reducibility. However, stabilization from the interaction with TiO_2 NTs is also crucial to enhance reducibility and likely to avoid sintering. Thus, at the end the active component is the hybrid system composed by TiO_2 nanotubes and small TiO_2 nanoparticles. Being in our experimental conditions, GO and GC the only two products of OX reduction detected (other products are in small traces, and also side H_2 formation is not significant in the best samples), changing the nature of this interaction between TiO_2 NTs and the supported TiO_2 (amorphous) nanoparticles also allow to tune the relative Faradaic selectivity to GC and GO.

A possible interpretation of these results is the following, although it is a tentative interpretation to offer a first mechanistic hypothesis, rather that a proof. The nature of the reduced titania species formed can be tentatively explained by considering the crystalline plane (101) of anatase phase, the most exposed on the surface, where an oxygen atom is bridging two Ti atoms, one with coordination number sixth and the other with coordination number five. Once this oxygen is removed, Ti changes its coordination number to 5 and 4, respectively, and the Ti^{4+} is reduced to Ti^{3+} by electron transfer in the 3d orbitals, obtaining a Ti_2O_3 like species. In TiO_2, oxygen vacancies from the bulk or surface causes one or two free electrons. In this way, the place occupied by the O^{2-} anion in the lattice is taken by these free electrons in the defective crystal and the energetic cost of the vacancy formation is minimized [53]. These electrons have a direct effect on the electronic structure of TiO_2 by forming a donor level at 0.7 eV below the bottom conduction band [54]. It is reported that effects associated with oxygen vacancies can alter the adsorption of some small molecules as CO, N_2O, H_2O, H_2, O_2, HCOOH, promoting dissociative over molecular adsorption [53,55]. It is thus reasonable to expect that these oxygen vacancies also play a role in activating in a similar way also OX, thus leading to the enhanced activity.

4.2. Comparison with literature results

With respect to earlier finding by Zhao et al. [18] using a roughened TiO_2 film electrode, apart that lower applied voltages are necessary in our case (2.9-3.4 V were used by Zhao et al. [18] possibly for the low conductivity of their electrodes, as confirmed from the long reaction times they used), we observed GC as the main product (in the best sample, TiNT-T) rather than GO,

moreover a correlation between OX conversion and selectivity to GC was demostrated. On the other hand, GO is intermediate to GC (Scheme 1) and thus it is well rational that an electrode with very low activity is necessary to stop to this intermediate. While GO is a product with higher added value than GC (around twice), electrode activity is equally crucial for the industrial development. From the practical perspective, data presented here show that two classes of electrodes prepared by anodic oxidation could be indicated. TiNT-T, where a pre-calcination step of Ti starting foil is made, giving higher OX conversion and GC yield, and a "conventional" preparation by anodic oxidation (TiNT), showing lower activity (but still acceptable) and coproducting GO and GC in similar amounts, but with a slightly prevalence of the former. Thus, by changing the electrode, it is possible to have a process, where the GC to GO ratio is changed depending on market requests.

These results are in agreement with those obtained recently by Yamamuchi et al. [56] who studied Ti-Zr oxide particles as electrodes for GC synthesis by OX electrocatalytic reduction, not using a full electrocatalytic cell, bur rather CV and chronoamperometry tests at 50°C. They conclude that amorphous rather than crystalline oxide is required in order to obtain better electrocatalytic performances. Atomic disordering would likely stabilize the formation of oxygen vacancies, and reducibility of the oxide, although characterization data on these aspects were not provided. Yamamuchi et al. [56] also showed that the less active samples show enhanced GO formation, while GC is maximized in the most active ones. Due to differences in the experimental campaign , a direct comparison of the datas is not possible, but their results obtained with Ti–ZrO_2 particle are well in line with those presented in Figure 5.

The same research group [57] investigated also the light-assisted electrochemical OX reduction (in the presence of external bias) using a TiO_2 cathode and a WO_3 photoanode obtaining 80% of FEs (FE_{GC} + FE_{GO}) applying a potential of 1.5 V vs. RHE under UV-visible irradiation ($\lambda >$ 300 nm) at 50 °C for 2 h. The cathode was prepared by depositing TiO_2 nanoparticles over a Ti foil, but robustness of this type of electrodes is weak and as indicated by authors also reaction rates were low (few $\mu mol \cdot h^{-1}$), around two-three order of magnitude lower than those we observed.

Recently Yang et al. [58] using multi-walled carbon nanotubes (MWNT) wrapped by an anatase TiO_2 layer, reported an OX conversion and GC selectivity of 51.2% and 38.7%, respectively at an applied potential of -2.2V vs RHE and 60 °C. The maximum reported yield in GC is thus around 19%, well in line with that we reported (Figure 7), but at room temperature rather than

60°C and not using an expensive anode electrode (IrO_2) as used by them. In addition, they did not report the formation of GO, considering that GC is the dominant product and its Faradaic selectivity is only about 40%, which indicates a significant formation of H_2 as side product.

Sadakiyo et al. [59] developed a PEAEC (polymer electrolyte alcohol electrosynthesis cell) containing porous TiO_2 obtained by hydrothermal synthesis, on a Ti felt as a cathode, obtaining nearly complete OX conversion and 31.9% FE_{GC} at 3.0 V applied voltage at 60 °C. However, the maximum energy conversion efficiency was less than 50%. Furthermore, the dominat product in terms of FE in these conditions was H_2, with FE around 60%. Specific current density to GC is about 20 $mA \cdot cm^{-2}$ which well compares with around 10 $mA \cdot cm^{-2}$ values we obtained but at room temperature and application of a lower potential. In addition, Sadakiyo et al. [59] results show a lowering of the current density in already 2h of tests.

These literature results are thus obtained at higher potentials and with greater energy consumption. The present work thus demonstred the possibility of a green synthetic process for the production of an alcoholic compound from an organic acid assisted by water electrolysis at the low potential of -1.1 V vs Ag/AgCl (-0,78 vs. RHE) and room temperature.

5. Conclusions

The analysis of the characteristics and reactivity of a series of electrodes prepared by anodic oxidation of Ti foils provide indications about the nature of the active species for the electrocatalytic reduction of oxalic acid to glycolic acid. These electrodes are robust and less toxic with respect to lead electrodes mostly studied in this reaction. They can be also prepared with low cost procedures which can be scaled-up. They do not need high potentials to operate efficienctly and the compared with literature results demonstrates the possibility of a green, renewable energy driven, process for the production of an alcoholic compound from an organic acid at the low potential of -1.1 V vs Ag/AgCl (-0,78 vs. RHE) at room temperature, not using critical raw materials and expensive or toxic electrodes. Coupled with an electrochemical synthesis of the oxalic acid from CO_2 the process represents a new green and low-carbon path to produce added value chemicals from CO_2.

The electrodes investigated have different characteristics. TiNT-A shows the presence of a dense nanostructured TiO_2 layer, without the presence of TiO_2 nanotubes. TiNT and TiNT-T, and TiNT-HS used as alternative preparation leading to nanotubes also without an ordered

packing, show the presence of amorphous small patches, debris or TiO_2 nanoparticles together with the TiO_2 nanotubes. They differ in terms of the characteristics of these amorphous TiO_2 nanoparticles, and the differences could be related to the details of the preparation procedure, with the anodization curves (Figure 1) providing good indications about the formation mechanism.

A series of relationships between the characteristics of these samples, in particular the concentration of oxygen vacancies (O2) and the amount of Ti^{3+} detected in XPS or the intensity of the anodic peak in CV tests, and the catalytic behavior (OX conversion and yield of GC, Y_{GC}) evidence the relation between these aspects. The analysis of the results indicate that in small amorphous TiO_2 nanoparticles (or surface pathces or debris) stabilized by interaction with TiO_2 NTs the sites responsible for the conversion of OX and GC yield. By varying this structural characteristic of the electrodes, it is possible to tune the GC to GO relative ratio.

Acknowledgments

This project has received funding from the European Union's Horizon 2020 research and innovation program under grant agreement ID 767798 (OCEAN). This MIUR PRIN 2017 project CO2 ONLY project nr. 2017WR2LRS gratefully acknowledged.

References

1. A. Mustafa, B. G. Lougou, Y. Shuai, Z. Wang, H. Tan, J. Energy Chem., 49 (2020) 96-123.
2. D. Saygin, D. Gielen, Energies 2021, 14, 3772.
3. R. S. Norhasyima, T. M. I. Mahlia, J. CO_2 Utiliz., 26 (2018) 323–335.
4. P. Lanzafame, S. Abate, C. Ampelli, C. Genovese, R. Passalacqua, G. Centi, S. Perathoner, ChemSusChem 10 (2017) 4409-4419.
5. S. Perathoner, G. Centi, Catal. Today 330 (2019) 157–170.
6. J. Huang, T. Yang, K. Zhao, S. Chen, Q. Huang, Y. Han, J. Energy Chem., 62 (2021) 71-102.
7. W. Zhu, K. Zhao, S. Liu, M. Liu, F. Peng, P. An, B. Qin, H. Zhou, H. Li, Z. He, J. Energy Chem., 37, (2019) 176-182.
8. Y. Zheng, A. Vasileff, X. Zhou, Y. Jiao, M. Jaroniec, S.-Z. Qiao, J. Am. Chem. Soc., 141

(2019) 7646–7659.
9. L. Fan, C. Xia, F. Yang, J. Wang, H. Wang, Y. Lu, Sci. Adv., 6 (2020) eaay3111.
10. E. Boutin, M. Robert, Trends in Chem., 3 (2021) 5.
11. M. A. Murcia Valderrama, R. J. van Putten, G. J. M. Gruter, Eur. Polym. J. 119 (2019) 445–468.
12. J. Iglesias, I. Martínez-Salazar, P. Maireles-Torres, D. Martin Alonso, R. Mariscal, M. López Granados, Chem. Soc. Rev., 49 (2020) 5704-5771.
13. A C. Garcia, C. Sanchez-Martinez, I. Bakker, E. Goetheer, ACS Sustainable Chem. Eng., 8 (2020) 10454-10460.
14. J. R. Ochoa, A. de Diego, J. Santa-Olalla, J. Appl. Electrochem., 23(1993) 905-9.
15. Y.-L. Zhou, X.-S. Zhang, Y.-C. Dai, W.-K. Yuan, Chem. Eng. Science, 58 (2003)1021-1027.
16. J. Li, X. Hu, Y. Su, Q. Li, Chem. Eng. Sci. 62 (2007) 6784–6793.
17. S. Masaaki, H. Shinichi, C. Xuedong, Y. Miho, S. Masaaki, Y. Miho. Sci. Rep., 7 (2017) 17032.
18. F. Zhao, F. Yan, Y. Qian, Y. Xu, C. Ma, J. Electroanal. Chem. 698 (2013) 31–38.
19. F. De, Luca, R. Passalacqua, F. P. Abramo, S. Perathoner, G. Centi, S. Abate, Chem. Eng. Trans., 84 (2021) 37-42.
20. X. Nie, S. Yin, W. Duan, Z. Zhao, L. Li, Z. Zhang, Nano, 16 (2021) 2130002.
21. Q. Zhou, Z. Fang, J. Li, M. Wang, Microporous and Mesoporous Mater., 202 (2015) 22-35
22. K. Lee, A. Mazare, P. Schmuki, Chem. Rev., 114 (2014) 9385-9454.
23. C. A.Grimes, J. Mater. Chem., 17 (2007) 1451-1457.
24. G. Centi, S. Perathoner, Eur. J. Inorg. Chem., 26 (2009) 3851-3878.
25. R. Passalacqua, S. Perathoner, G. Centi, Catal. Today, 251 (2015) 121-131.
26. G. Centi, S. Perathoner, Coord. Chem. Rev. 255 (2011) 1480-1498.
27. C. Ampelli, R. Passalacqua, S. Perathoner, G. Centi, D. S. Su, G. Weinberg, Topics in Catal., 50 (2008) 133-144.
28. R. Passalacqua, C. Ampelli, S. Perathoner, G. Centi, Nanosci. and Nanotechn. Lett., 4 (2012) 142-148.
29. G. Centi, R. Passalacqua, S. Perathoner, Mater. Sci. in Semiconductor Proc., 42 (2016) 115-121.
30. K. C. Sun, M. B. Qadirm, S. H. Jeong, RSC Adv., ,4 (2014) 23223-23230.
31. A, Nakahira, T. Kubo, C. Numako, Inorg. Chem., 49 (2010) 5845–5852.
32. S. Du, Engineering, 7 (2021) 33-49.

33. Md. Z. H. Khan, X. Liu, J. Electronic Mater., 48 (2019) 4148-4165.
34. M. Madian, A. Eychmueller, L. Giebeler, Batteries, 4 (2018) 7/1-36.
35. Y. Zhang, Y. Tang, W. Li, X. Chen, ChemNanoMat, 2 (2016) 764-775.
36. T. Berger, D. Monllor-Satoca, M. Jankulovska, T. Lana-Villarreal, R. Gomez, ChemPhysChem, 13 (2012) 2824-2875.
37. G. Centi, R. Passalacqua, S. Perathoner, D. S. Su, G. Weinberg, R. Schlögl, Phys. Chem. Chem. Phys. 9 (2007) 4930–4938.
38. A. Apolinário, P. Quitério, C. T. Sousa, J. Ventura, J. B. Sousa, L. Andrade, A. M. Mendes, J. P. Araújo, J. Phys. Chem. Lett., 6 (2015) 845–851.
39. P. Roy, S. Berger, P. Schmuki, Angew. Chemie - Int. Ed., 50 (2011) 2904–2939.
40. S. P. Albu, P. Roy, S. Virtanen, P. Schmuki, Isr. J. Chem. 50 (2010) 453–467.
41. J. M. Macak, S. P. Albu, P. Schmuki, Phys. Status Solidi - Rapid Res. Lett., 1 (2007) 181–183.
42. M. Moazeni, H. Hajipour, M. Askari, M. Nusheh, Mater. Res. Bull. 61 (2015) 70–75.
43. V.A. Sugiawati, F. Vacandio, A. Galeyeva, A.P. Kurbatov, T. Djenizian, Front. Phys., 7 (2019) 179.
44. F. Fabregat-Santiago, I. Mora-Seró, G. Garcia-Belmonte, J. Bisquert, J. Phys. Chem. B, 107 (2003) 758–768.
45. H. Yu, J. Ma, Y. Zhang, X. Zhang, W. Shi, Electrochimica Acta, 56 (2011) 6498-6502.
46. N. Makivić, J.-Y. Cho, K. D. Harris, J.-M. Tarascon, B. Limoges, V. Balland, Chem. Mater., 33 (2021) 3436–3448.
47. S. Bellamkonda, N. Thangavel, H. Y. Hafeez, B. Neppolian, G. Ranga Rao, Catal. Today 321–322 (2019) 120–127.
48. Z. Li, H. Bian, X. Xiao, J. Shen, C.o Zhao, J. Lu, Y. Li, ACS Appl. Nano Mater., 2 (2019) 7372–7378.
49. B. Bharti, S. Kumar, H. N. Lee, R. Kumar, Sci. Rep. 6 (2016) 1–12.
50. X. Zhang, H. Tian, X. Wang, G. Xue, Z. Tian, J. Zhang, S. Yuan, T. Yu, Z. Zou, Mater. Lett. 100 (2013) 51–53.
51. H. Xua, Q. Zhang, C. Zheng, W. Yan, W. Chu, Appl. Surface Sci., 257 (2011) 8478–8480.
52. W. A. Abbas, I. H. Abdullah, B. A. Ali, N. Ahmed, A. M. Mohamed, M. Y. Rezk, N. Ismail, M. A. Mohamed, N. K. Allam, Nanoscale Adv., 1 (2019) 2801-2816.
53. X. Pan, M. Q. Yang, X. Fu, N. Zhang, Y. J. Xu, Nanoscale 5 (2013) 3601–3614.
54. C. Di Valentin, G. Pacchioni, A. Selloni, A. J. Phys. Chem. C, 113 (2009) 20543–20552.
55. D. N. Pei, L. Gong, A.-Y. Zhang, X. Zhang, J.-J. Chen, Y. Mu, H.-Q. Yu. Nat. Commun. 6 (2015) 2–11.
56. M. Yamauchi, S. Hata, H. Eguchi, S. Kitano, T. Fukushima, M. Higashi, M. Sadakiyo, K. Kato, Catal. Sci. Technol.,9 (2019) 6561-6565.
57. S. Kitano, M. Yamauchi, S. Hata, R. Watanabe, M. Sadakiyo, Green Chem. 18 (2016) 3700–3706.
58. J. Yang, J. Cheng, J. Tao, M. Higashi, M. Yamauchi, N. Nakashima, ACS Appl. Nano

Mater., 2 (2019) 6360–6367.
59. M. Sadakiyo, S. Hata, X. Cui, M. Yamauchi, Sci. Rep. 7 (2017) 1–9.

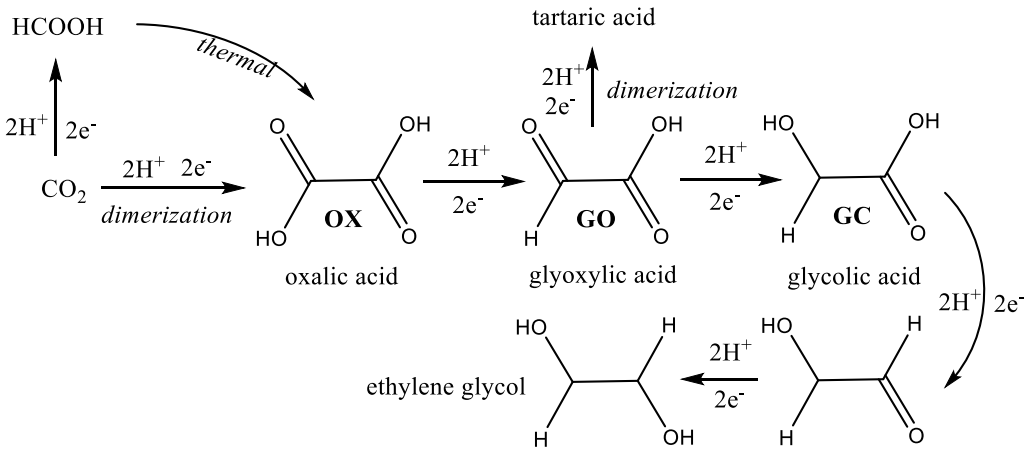

Scheme 1. Simplified reaction newtwork in the electrocatalytic conversion of CO_2 to C2 high added value chemicals.

Table 1. Overview of the samples prepared and the acronym used.

Name	*Pre-treatment*	*Aging time (minutes)*	*Method*
TiNT	None	60	Anodic oxidation
TiNT-A	None	240	Anodic Oxidation
TiNT-T	Calcination	60	Anodic Oxidation
TiNT-HS	None	-	Hydrothermal synthesis

Table 2. Binding energies (eV) of Ti2p and O1s peaks present in the XPS spectra of TiNT samples and the corresponding percentage of oxygen vacancies (O2) and Ti^{3+}.

	Ti^{4+}(eV)		*Ti^{3+}(eV)*		*O (eV)*		*Total percentage*	*Total percentage*	*OX $Conv_{avg}$(%)*
Sample	Ti2p3/2	Ti2p1/2	Ti2p3/2	Ti2p1/2	O1	O2	O2	Ti^{3+}	
TiNT	458.67	464.21	456.95	462.49	530.05	531.87	7.00	5.14	6.81
TiNT-A	458.45	463.99	456.88	462.42	529.64	531.70	6.80	5.11	6.62
TiNT-HS	458.50	464.04	456.91	462.45	529.81	531.32	14.70	5.54	26.00
TiNT-T	458.60	464.14	456.95	462.49	529.90	531.31	19.00	5.71	32.00

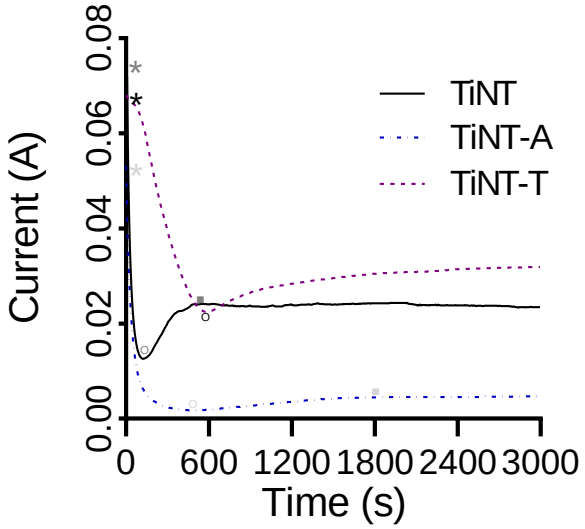

Figure 1. Current versus time during the anodic oxidation (50 V, 1 hour; *,o, ▪ indicate I_0,I_{min} and I_{max}, respectively)

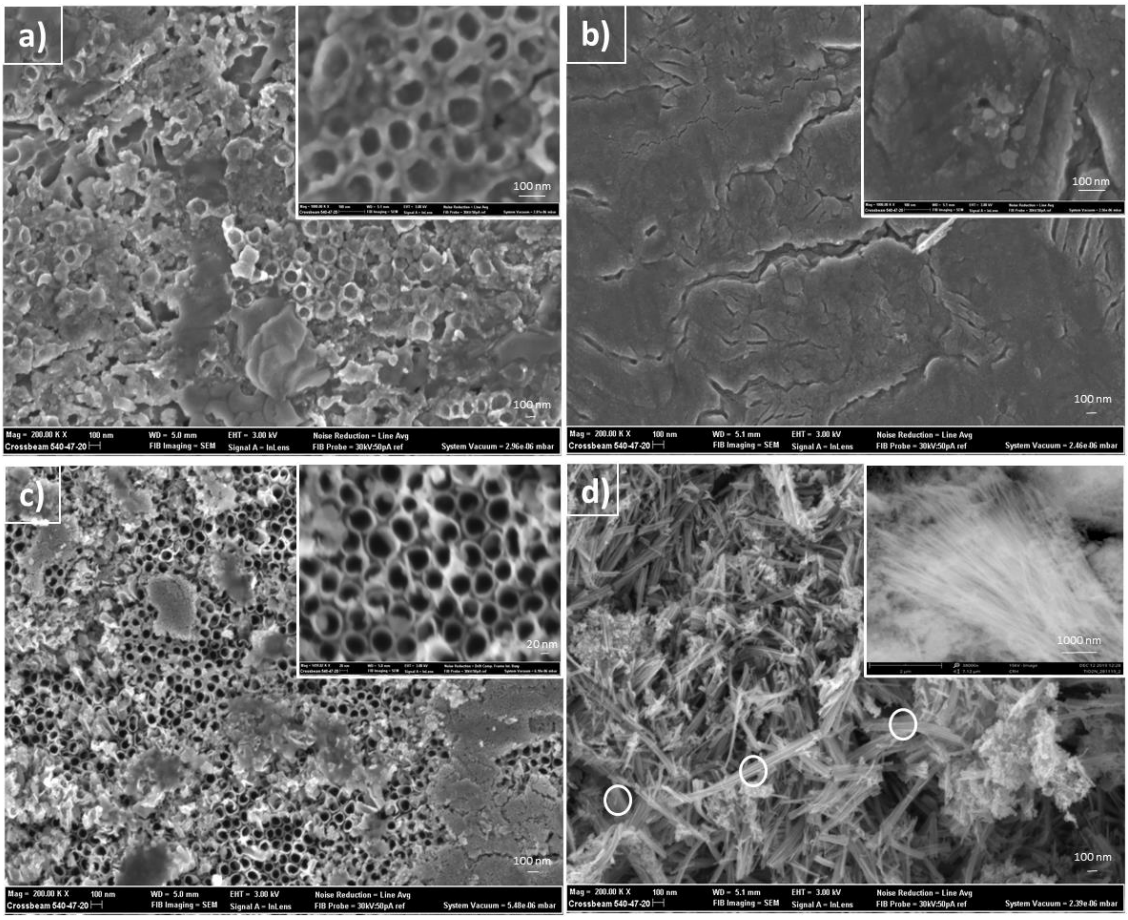

Figure 2. SEM top-view mages of the electrodes: a) TiNT, b) TiNT-A, c) TiNT-T, d) TiNT-HS. Insets show higher magnification micrographs.

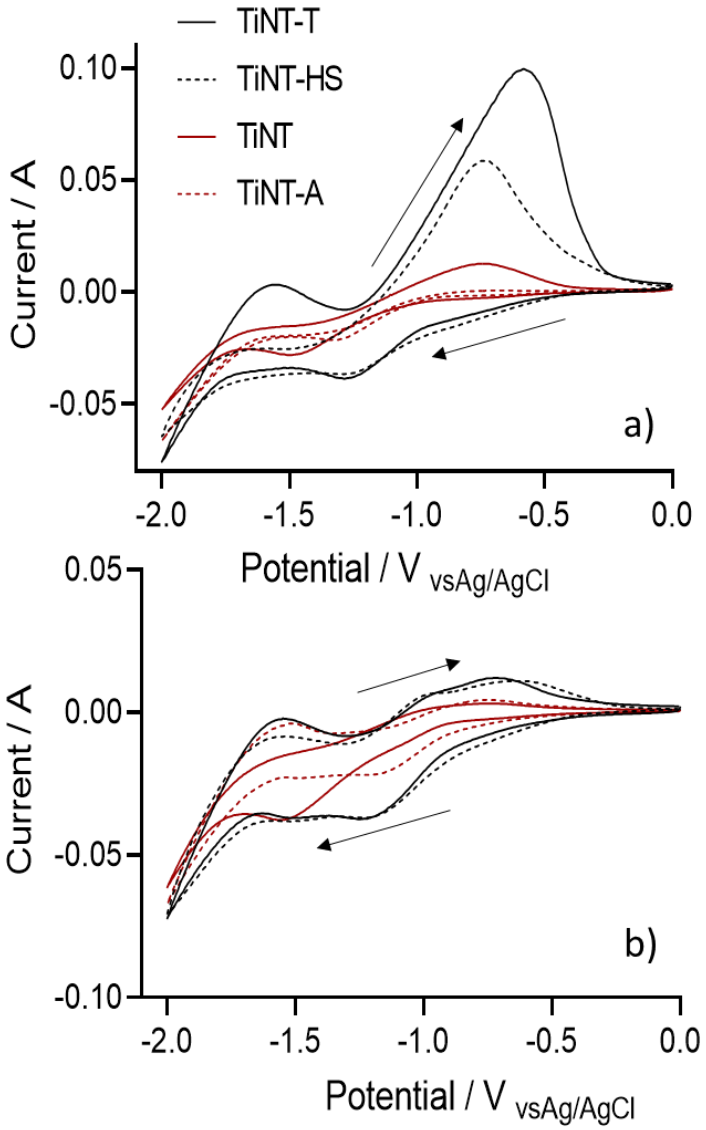

Figure 3. Cyclic Voltammetry a) in Na_2SO_4 0.2 M and b) adding an Oxalic acid solution 0.03 M

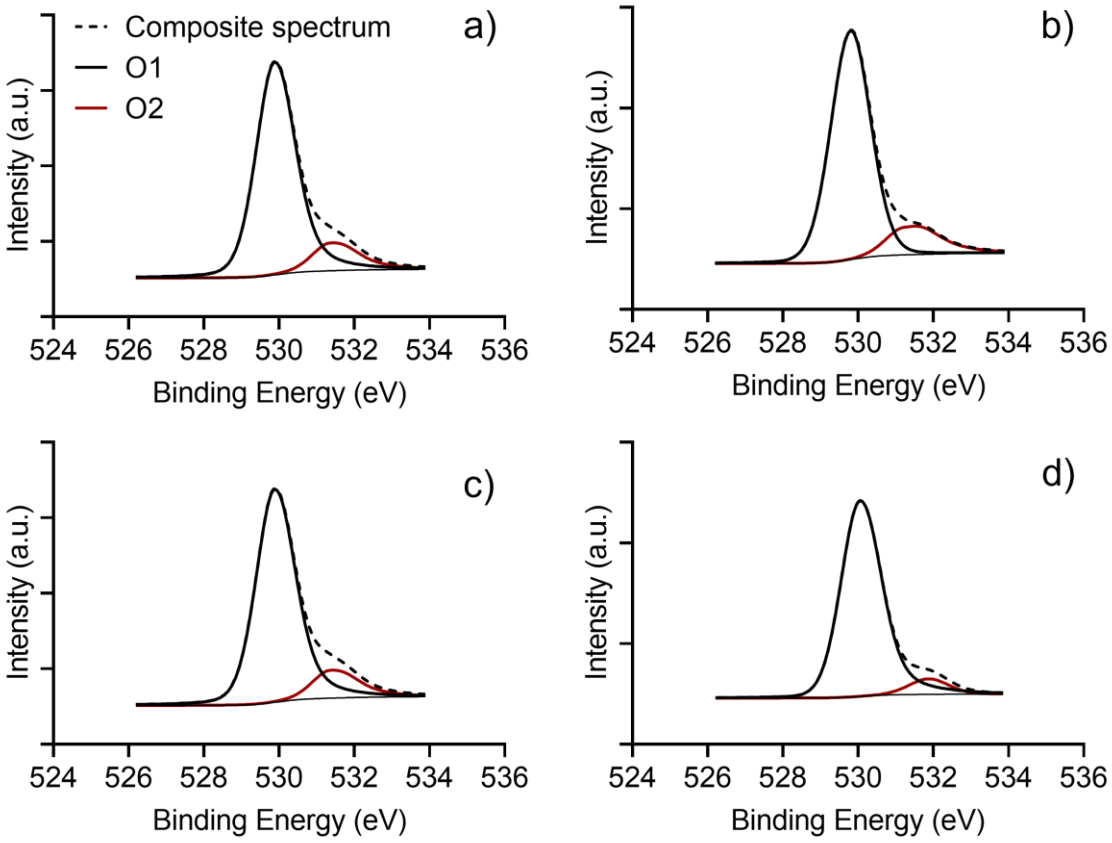

Figure 4. O1s photoemission spectra of a) TiNT-T, b) TiNT-HS, c) TiNT and d) TiNT-A

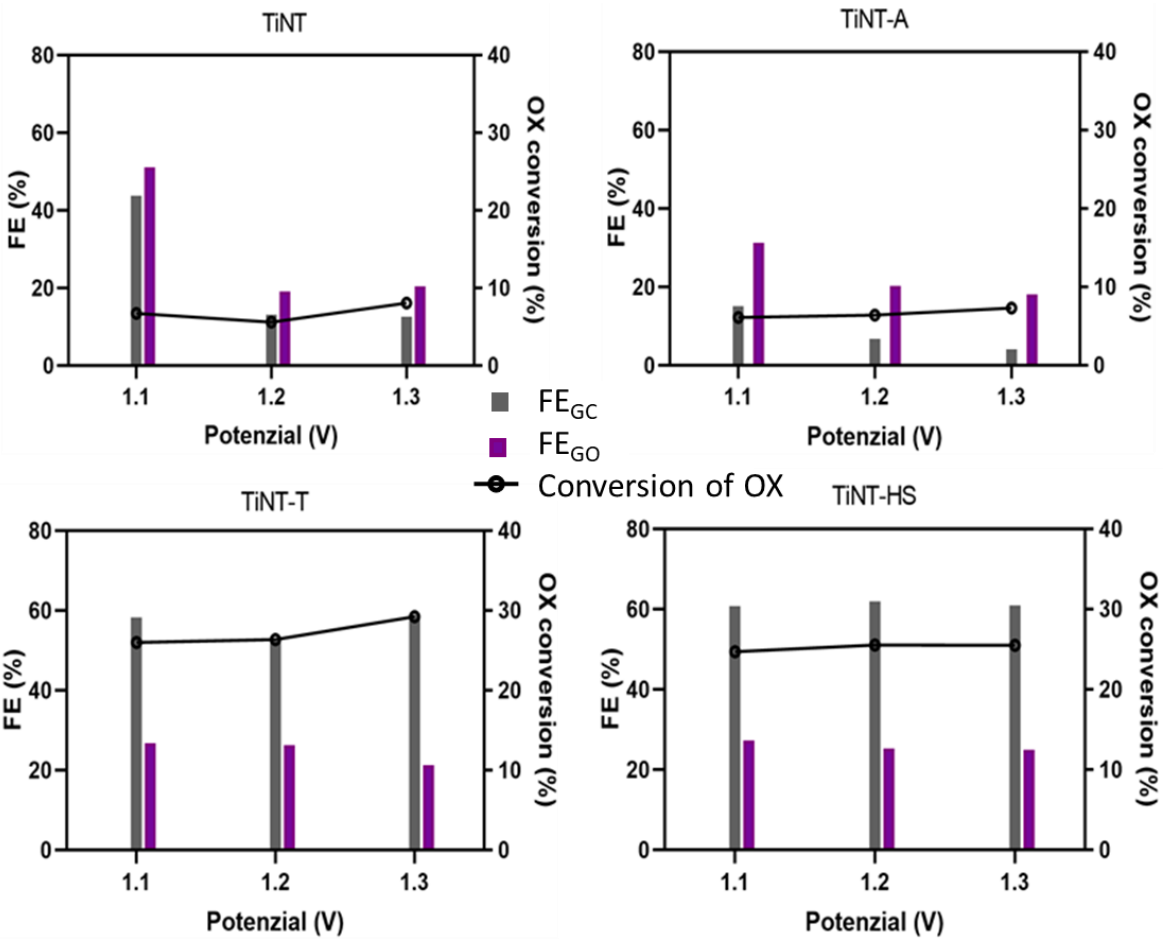

Figure 5. Faradaic efficiency (EF) and conversion of OX at three potential investigated (-1.1; -1.2; -1.3) for the TiNT, TiNT-A, TiNT-T and TiNT-HS electrodes.

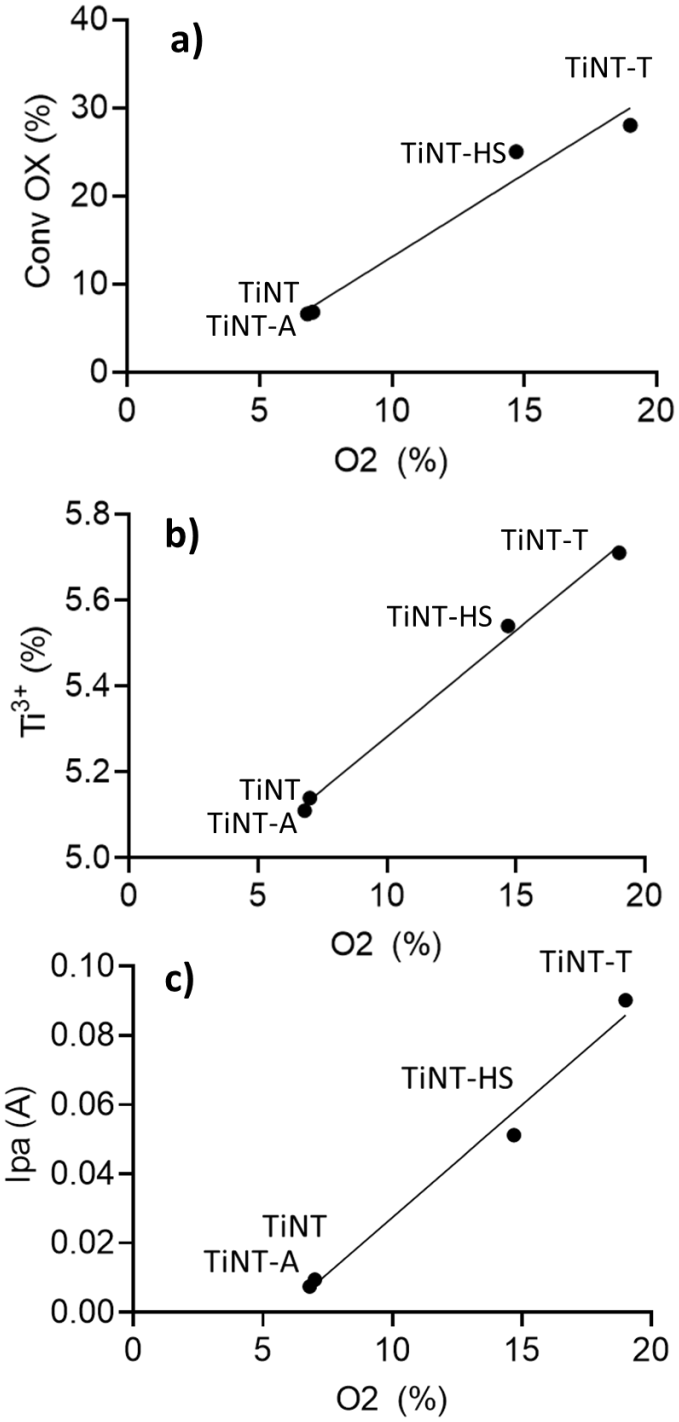

Figure 6. Linear relationships obserbed in the series of TiNT electrodes between O2 (oxygen vacancies measured by XPS) percentage and (a) conversion of oxalic acid (OC), b) concentration of Ti^{3+} determined by XPS, and c) an Ipa (peak intensity in CV tests for the anodic peak in the range -0.8 ÷ -0.9 V).

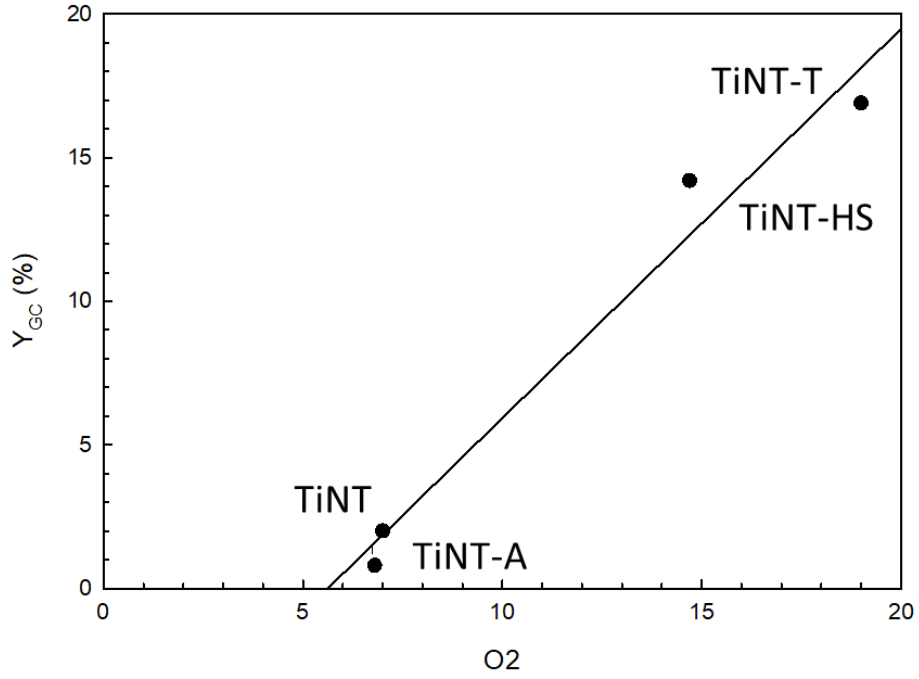

Figure 7. Relationships observed in the series of TiNT electrodes between O2 (oxygen vacancies measured by XPS) percentage and yield of GC (Y_{GC}, %) for tests at -1.3 V.

Electrocatalytic production of glycolic acid from CO_2 via oxalic acid reduction on titania debris supported on a TiO_2 nanotube array

Francesco Pio Abramo[a], Federica De Luca[a], Rosalba Passalacqua[a], Gabriele Centi[a], Gianfranco Giorgianni[b], Siglinda Perathoner[a], Salvatore Abate[a,*]

[a] *Department of ChiBioFarAM (Industrial Chemistry), University of Messina, ERIC aisbl and INSTM/CASPE, V.le F. Stagno d'Alcontres 31, Messina 98166, Italy*

[b] *University of Calabria, Department of Environmental Engineering, Laboratory of Industrial Chemistry and Catalysis Via P. Bucci, 87036 Rende (CS), Italy*

SUPPORTING INFORMATION

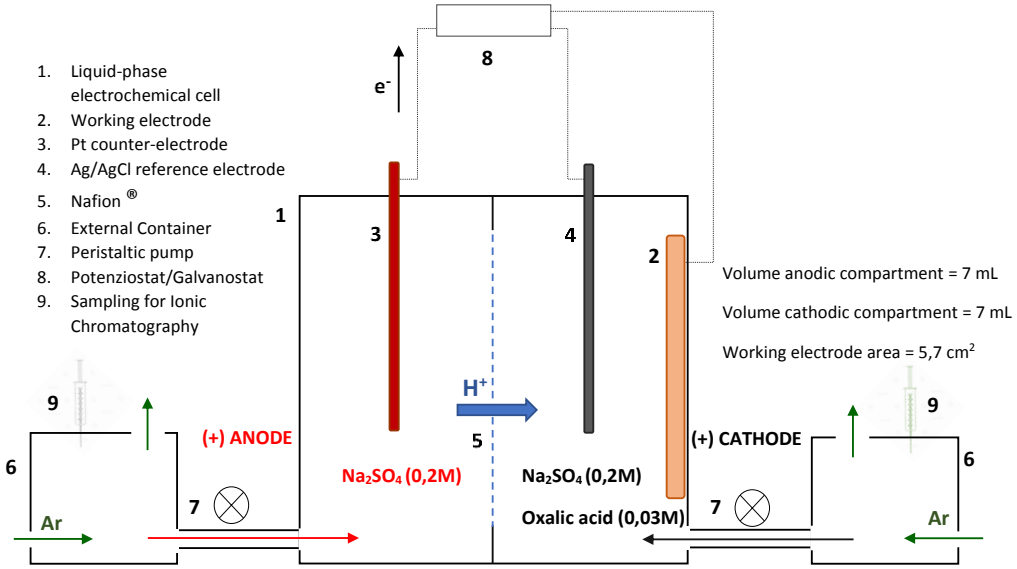

Figure S1. Experimental apparatus

The electro-catalytic cell is divided into two compartments: (1) anodic and (2) cathodic with the proton-exchange membrane (Nafion® 117) acting as the partition. A 0.2 M Na_2SO_4 solution with OX (oxalic acid) 0.03 M (pH=2) is used to perform the reaction in the cathodic compartment, while the electrolyte solution (0.2M Na_2SO_4) is used for the anodic compartment. In the latter, the pH was adjusted adding small amounts of a 1 M H_2SO_4 solution, to get the same pH of the cathode side. The external reservoirs (6) containing the electrolytic solutions are flowed with Argon (20 ml/min) for 30 minutes in order to push the O_2 out, before starting the reaction. The electrolytic solutions are flushed to both the compartments by using a peristaltic pump (7). The solution volume (cathode + external tank + tubes) is 35 ml and the net volume in the cathodic compartment is 7 ml, the same as in the anode. The test was carried out for 2 hours for each investigated potential, the products were analyzed by Ionic Chromatography Metrohm, using 0.5 mM H_2SO_4 as mobile phase, with a flow of 0.5 mL/min, at an average pressure of 5 MPa, and as stationary phase a column for organic acids 25 cm long and with an internal diameter of 7.8 mm, preceded by a Metrosep Organic Acid Guard pre-column, 50 mm long and 4 mm thick. A 944 professional UV/vis Detector Vario at 215 nm was used to detect the products.

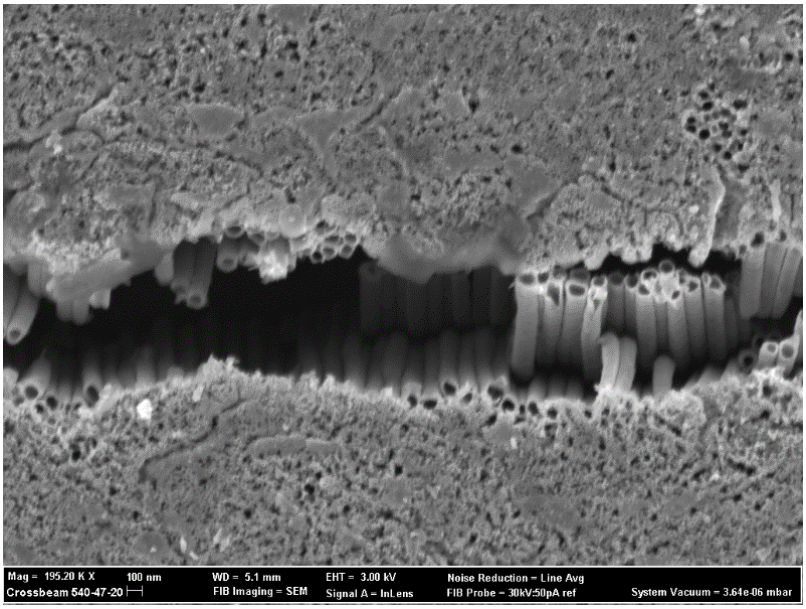

Figure S2. Close-up of a crack in the oxide layer of TiNT-T

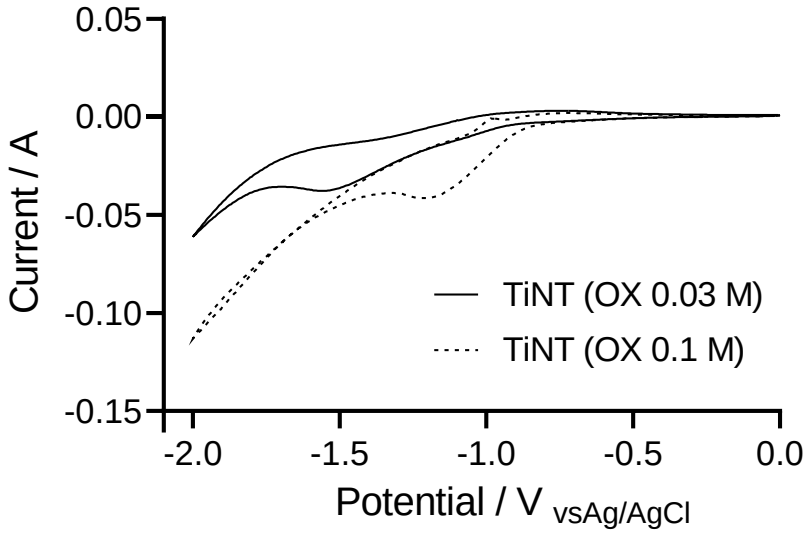

Figure S3. Cyclic voltammetry in an oxalic acid solution 0.01 M and 0.03 M for the TiNT sample

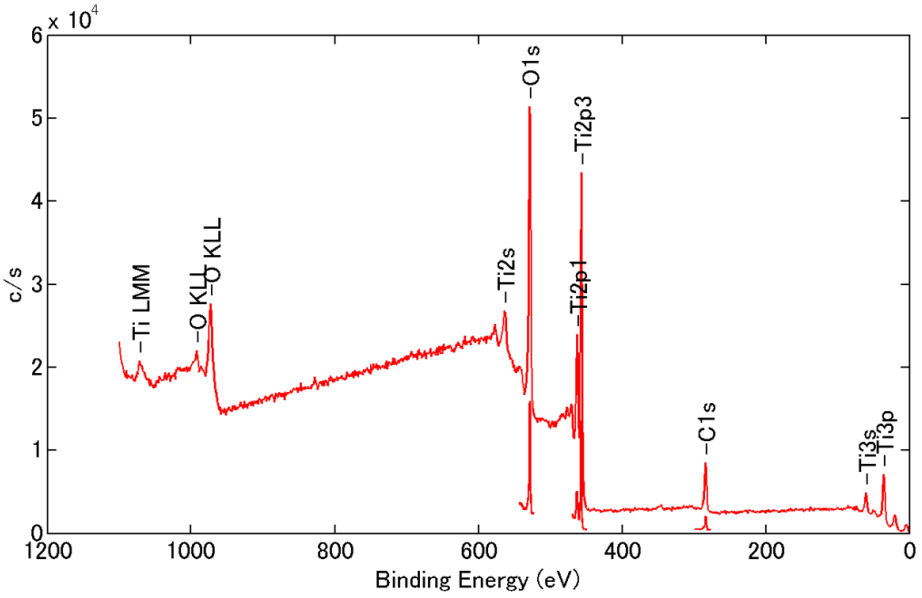

Figure S4. Survey XPS spectrum for TiNT-T sample

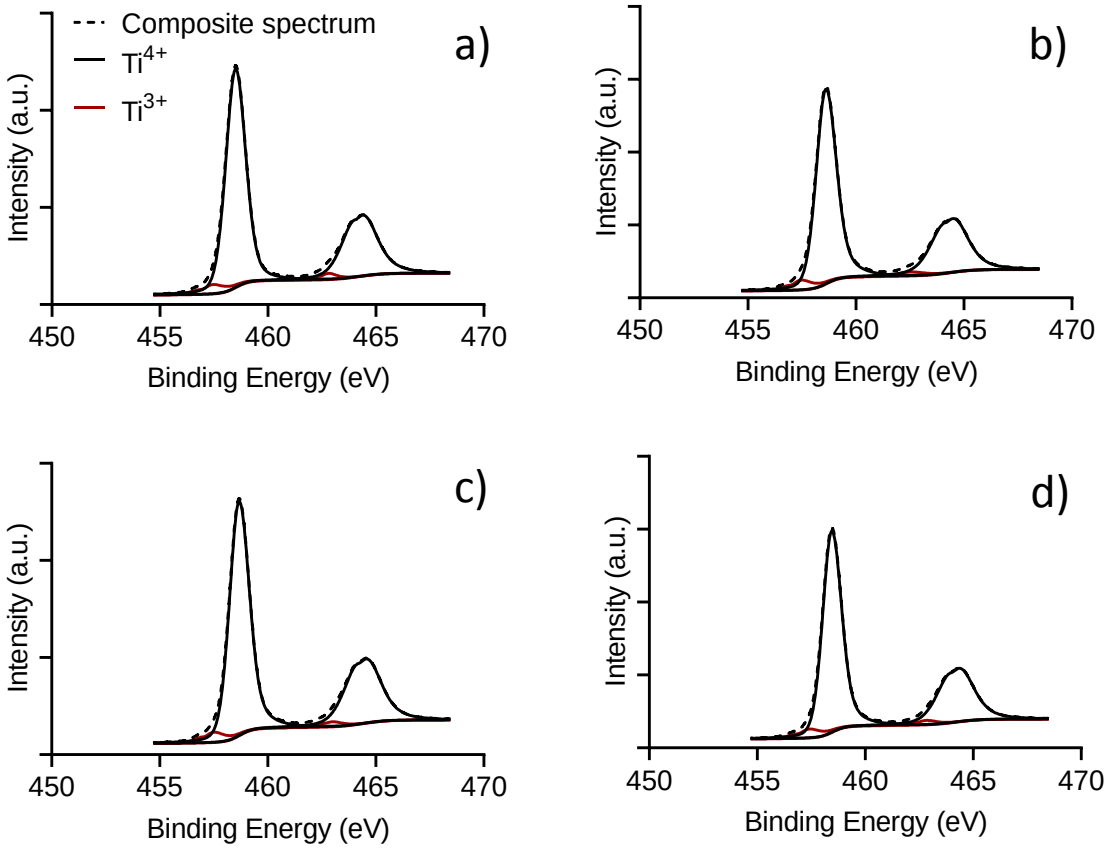

Figure S5. Ti2p photoemission spectra of a) TiNT-T, b) TiNT-HS, c) TiNT and d) TiNT-A.

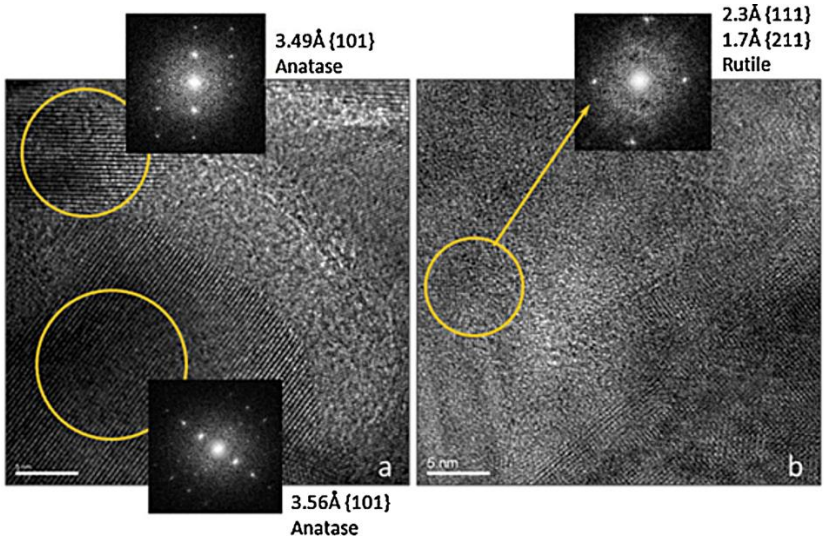

Figure S6. HRTEM micrographs of supported TiO_2 NTs (on Ti substrate) thermally annealed at 450 °C: (a) anatase phase at the top of the TiNT thin film array and (b) rutile phase of the bottom area at the interface between the oxide thin layer and the metallic substrate [1].

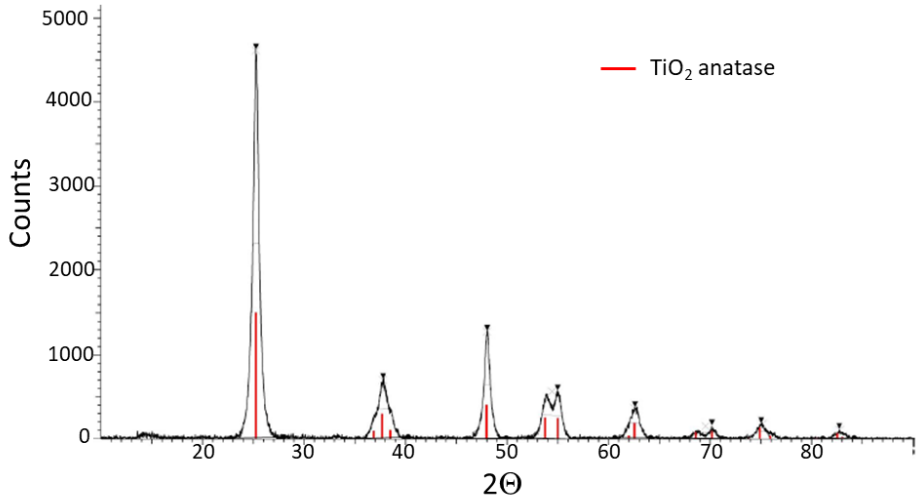

Figure S7a. X-ray diffraction pattern of TiNT-HS

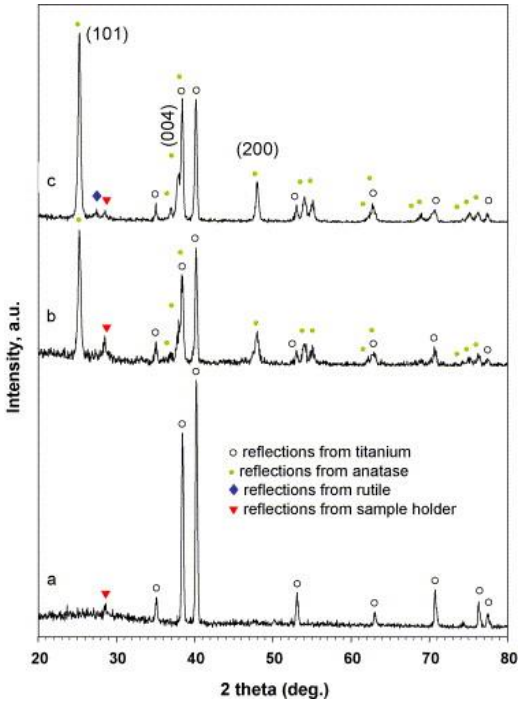

Figure S7b. GAXRD of TiNT after anodization (a), further annealing in air at 450 °C for 3 h (b) and 500 °C for 3 h (c) [1].

Glancing angle X-ray diffraction (GAXRD) measurements: the diffraction patterns of the samples were collected in the 20-80° 2θ range at a scan rate of 0.02°/s using a diffractometer (Philips X'Pert 3710 equipment) with monochromatic Cukα radiation (λ = 1.54178 Å) by applying an accelerating voltage and current of 40 kV and 30 mA, respectively. A glancing angle of 0.5° was used for all measurements.

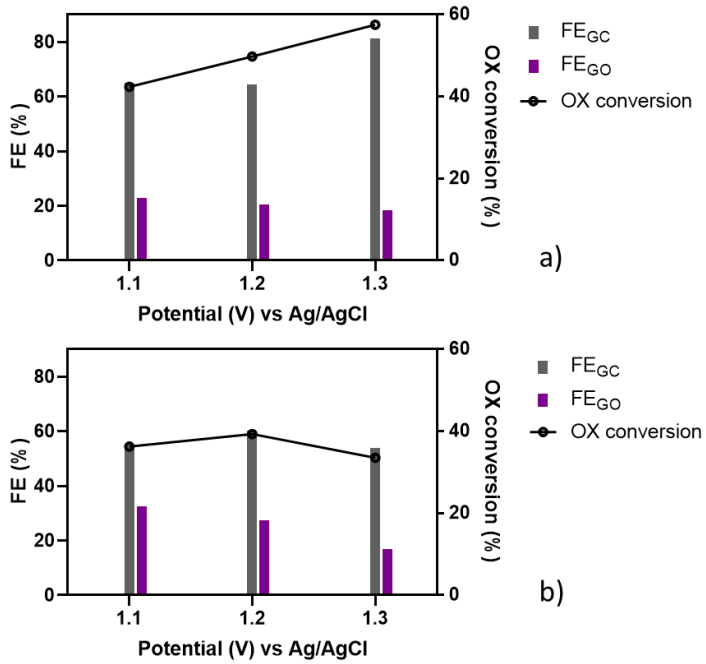

Figure S8. Electrocatalytic behaviour of an optimized TiNT sample a) before and b) after ultra-sonification treatment.

Table S1 Summary of the electrocatalytic results (2h of test at each condition). For definition of FE (Faradaic Efficiency), OX conversion and Y (yield) see text. $I_{average}$ is the average current density in 2h continuous tests.

Potential (V)		**-1.1 V vs. Ag/AgCl**				
Electrode	*FE_{GO} (%)*	*FE_{GC} (%)*	*OX conv. (%)*	*Y_{GO} (%)*	*Y_{GC} (%)*	*$I_{average}$ (mA/cm^2)*
TiNT	51,9	44,5	6,8	4,7	2,1	-8,1
TiNT-A	31,2	15,1	6,1	4,9	1,2	-14,0
TiNT-T	32,8	71,0	26,1	12,5	13,5	-10,1
TiNT-HS	27,3	69,8	24,7	11,5	13,2	-11,4
Ti-T	10,8	5,6	4,1	3,2	0,9	-0,9
Potential (V)		**-1.2 V vs. Ag/AgCl**				
Electrode	*FE_{GO} (%)*	*FE_{GC} (%)*	*OX conv. (%)*	*Y_{GO} (%)*	*Y_{GC} (%)*	*$I_{average}$ (mA/cm^2)*
TiNT	19,4	13,3	5,6	4,1	1,5	-19,1
TiNT-A	20,3	6,7	6,4	5,5	0,9	-24,1
TiNT-T	34,0	67,5	26,4	12,6	13,7	-10,3
TiNT-HS	25,2	61,9	25,6	11,3	14,2	-12,1
Ti-T	5,3	1,4	2,9	2,5	0,3	-1,4
Potential (V)		**-1.3 V vs. Ag/AgCl**				
Electrode	*FE_{GO} (%)*	*FEGC (%)*	*OX conv. (%)*	*Y_{GO} (%)*	*Y_{GC} (%)*	*$I_{average}$ (mA/cm^2)*
TiNT	22,7	14,1	8,1	6,1	2,0	-24,0
TiNT-A	18,0	4,0	7,3	6,5	0,8	-32,3
TiNT-T	28,3	68,5	28,8	11,9	16,9	-12,2
TiNT-HS	25,0	61,0	25,5	11,3	14,2	-12,2
Ti-T	8,3	0,0	3,9	3,9	0,0	-1,5

Reference

1. (a) S. Perathoner, R. Passalacqua, G. Centi, D. S. Su, G. Weinberg, Catal. Today, 122 (2007) 3-13. (b) R. Passalacqua, S. Perathoner, G. Centi, Catal. Today, 251 (2015) 121-131.